In–situ observations of waves in Venus' polar lower thermosphere with Venus Express aerobraking

Ingo C. F. Müller-Wodarg[1], Sean Bruinsma[2], Jean-Charles Marty[2] & Håkan Svedhem[3]

[1]*Blackett Laboratory, Imperial College London, Prince Consort Road, London SW7 2AZ, UK.*

[2]*CNES/GRGS, 18 Avenue E. Belin, F-31401 Toulouse Cedex 9, France.*

[3]*ESA/ESTEC, Postbus 299, 2200 AG Noordwijk, The Netherlands.*

Waves are ubiquitous phenomena found in oceans and atmospheres alike. From earliest formal studies of waves in the Earth's atmosphere to more recent studies on other planets, waves have been shown to play a key role in shaping atmospheric bulk structure, dynamics and variability[1–4]. Yet, waves are difficult to characterise as they ideally require *in-situ* measurements of atmosphere properties which are difficult to obtain away from Earth. Thereby, we have incomplete knowledge of atmospheric waves on planets other than our own, and we are thereby limited in our ability to understand and predict planetary atmospheres. We report on the first ever *in-situ* observations of atmospheric waves in Venus' thermosphere (130–140 km) at high latitudes (71.5–79.0°). These were made by the Venus Express Atmospheric Drag Experiment (VExADE)[5] during aerobraking from June 24–July 11, 2014. As the spacecraft flew through Venus' atmosphere, deceleration by atmospheric drag was sufficient to obtain from accelerometer readings a total of 18 vertical density profiles. We infer an average temperature of T=114±23 K and findhorizontal wave-like density perturbations and mean temperatures being modulated at a quasi-5-day period.

Atmospheric total mass densities in Venus' lower thermosphere are inferred from accelerometer measurements made onboard the Venus Express (VEx) spacecraft on its polar and highly eccentric orbit ($e = 0.84$) with pericentre near 75°N at the terminator and 130–134 km altitude during the aerobraking phase from June 24 – July 11, 2014. This was the first and only aerobraking experiment carried out by the spacecraft, shortly before contact was lost on November 28, 2014. At each of the 18 consecutive days, one density profile extending about 3° in latitude on both sides of the pericentre (point of closest approach) was obtained. A summary of all density measurements is shown in the upper panel of Figure 1 as a function of spacecraft latitude. Each line in the figure represents densities measured during one flyby. Overall, the densities are largest near the pericentre latitude (75°N) due to the lowest altitude of the spacecraft there, and they decrease away from that latitude due to the increasing spacecraft altitude. In a hydrostatic isothermal atmosphere, the density change with altitude z is given by

$$\rho(z) \; = \; \rho(z_0) \; exp\left(-\frac{z - z_0}{H}\right) \tag{1}$$

where $\rho(z)$ and $\rho(z_0)$ are densities at altitudes z and z_0 (the pericentre altitude), and H is the atmospheric scale height which for simplicity we assume to be constant with height. In such an idealised case, $\rho(z_0)$ represents the largest density during any flyby, though in our data we find densities to not always be largest at pericentre due to strong background perturbations which are visible in Figure 1.

We may compare our densities to a commonly used empirical Venus upper atmosphere model, VTS3[6], which was produced from nearly 2 years (1978–1980) of continuous *in-situ* composition measurements at 142–250 km altitude by the Pioneer Venus Orbiter Neutral Mass Spectrom-

eter (PV-ONMS)[7]. While these observations were made near the equator (16°N) covering all local times (and all solar zenith angles), Venus' upper atmosphere was assumed to be forced primarily by solar heating and the PV-ONMS observations were extrapolated to polar latitudes by assuming the same solar zenith angle dependence identified at low latitudes from local time changes to apply when moving at any fixed local time from equator to pole. Our observations allow us to assess the validity of this assumption.

For each flyby, we produced an individual hydrostatic density fit, ρ_{fit}, which satisfies Equation 1 and represented a least mean square fit to observed densities, ρ, of that flyby. We determined for each density profile the combination of $\rho(z_0)$ and H values that produced the optimal ρ_{fit} profile. The dashed red lines in the upper panel of Figure 1 show two examples of such hydrostatic fits. As a result of producing these fits, we obtained 18 individual values of scale height, one per flyby, with a mean value of $H = 2.9 \pm 0.6$ km. Although temperatures are not directly measured by our experiment, we may use the derived scale heights with the definition $H = kT/(mg)$ to infer temperatures, T, for every flyby (k being the Boltzmann constant, $g = 8.49$ m/s^2 the gravity acceleration and m the mean molecular weight). We have no direct measurements of m from VEx but may estimate these from the VTS3 model. Over the latitude and local solar time (LST) ranges of our observations (71.5° – 79.0°N, 4.5 h – 6.3 h LST) as well as the range of solar flux during the relevant dates (F10.7$_{mean}$=130.7–134, F10.7$_{daily}$=93.4–200.7), VTS3 predicts m=34.7–41.8 atomic mass units (AMU), or an average of $m = 38.3$ AMU. From these inputs we obtain 18 temperature values, again one per flyby, with an average of $T = 114 \pm 23$ K. For the same locations and conditions, VTS3 temperatures range from 141–159 K, so our inferred

temperatures are considerably lower than values from VTS3. Our derived T values assumed the same m for all flybys, which adds a further systematic uncertainty of $\pm 10\%$ to our temperatures but will not change the basic finding of our temperatures being lower than those of VTS3. Recent observations by the Venus Express SPectroscopy for the Investigation of the Characteristics of the Atmosphere of Venus (SPICAV) and Solar Occultation in the InfraRed (SOIR) instruments found thermosphere temperatures at high latitudes near 130–140 km of around 120 K[8,9], consistent with our value. So, the VTS3 model appears to be over-estimating lower thermosphere temperatures at higher latitudes.

We may furthermore use the hydrostatic density profiles, ρ_{fit}, to extract the perturbations from the background densities in the atmosphere. This analysis assumes background densities to be close to the idealised hydrostatic fits, an approximation which is sufficiently accurate over the small vertical and horizontal range of sampled densities. The middle panel of Figure 1 shows normalised density perturbations, $(\rho - \rho_{fit})/\rho_{fit}$, to be of the order of 10%. They may be characterised as fairly regular wave pattern (visible in the top and middle panels of the figure), and we therefore interpret these as signatures of atmospheric waves.

The overall variability of measured densities is also visible in Figure 2 which displays all measured densities versus altitude. The red crosses show averages taken over bins spaced vertically by 2.5 km. The red line is a hydrostatic density curve with a slope defined by the previously obtained average scale height of $H = 2.9$ km. We centred the red line around the average density value at 133.5 km and find that it passes fairly well also through the other two average values (red

crosses), so the line captures well the overall slope of the profiles, confirming the validity of our previously described approach in determining H via the ρ_{fit} profiles.

Blue crosses in Figure 2 are averages of densities from the VTS3 model that were sampled at the identical locations and conditions as those we measured and illustrate that measured densities are smaller by around 22% near 130 km and 40% near 140 km with respect to those of VTS3. Linearly extrapolating this trend upward to 180 km altitude would imply a discrepancy by a factor of around 2 there, in agreement with the discrepancy found by VExADE via Precise Orbit Determination at higher altitudes (176–186 km)[10]. This suggests scale heights in Venus' polar atmosphere to be systematically lower than predicted by VTS3 above around 100 km. This is consistent with our earlier finding of Venus' polar upper atmosphere being cooler than predicted by VTS3. The broader significance of these differences is that the assumptions of solar zenith angle symmetry underlying VTS3 are too simplistic for high latitudes where other factors such as winds may lead to polar temperatures in the lower thermosphere being cooler than expected from solar forcing alone.

A second finding from Figure 2 is that variability in the VTS3 model densities is lower than that of measured densities. Over the altitude range of Figure 2 the average 1-σ variation of measurements (normalised to their background value) is 0.35, the corresponding value for VTS3 densities is 0.19. The local time changes, in particular, are responsible for most of the variability in VTS3 since the locations sampled in this study reach across the terminator where the upper atmosphere is known to change considerably[6,7]. The additional variability of our densities is caused

by the density waves that we identified in Figure 1.

To investigate these waves further, the upper and middle panels of Figure 3 show normalised values, $(\rho - \rho_{fit})/\rho_{fit}$, for June 30, 2014 (panel A) and July 07, 2014 (panel B) as a function of distance to the closest approach point. We chose these two days as examples stronger wave activity (Panel A) and weaker wave activity (Panel B). To quantify the amplitudes on each individual day, we fit the waves of every individual flyby with the sum of two wave trains, shown as dashed lines in panels A and B of Figure 3. The amplitudes and horizontal wavelengths of wave trains "1" and "2" are denoted by A_1, λ_1 and A_2, λ_2, respectively, and we obtained a single set of values for these at each flyby. Averaged over the 18 flybys, mean wavelengths are $\lambda_{1\text{ mean}} = 275 \pm 70$ km and $\lambda_{2\text{ mean}} = 126 \pm 30$ km and their mean amplitudes are $A_{1\text{ mean}} = 0.09 \pm 0.04$ and $A_{2\text{ mean}} = 0.07 \pm 0.03$, respectively. The similarity of $A_{1\text{ mean}}$ and $A_{2\text{ mean}}$ justifies our use of 2 wave trains. While we attempted fitting 3 wave trains, the amplitudes of the third wave were considerably smaller.

Values of $A_1/A_{1\text{ mean}}$ (blue dots) and $A_2/A_{2\text{ mean}}$ (blue triangles) are shown in the bottom panel of Figure 3 as a function of time (days from June 24, 2014). Thick markers on the x-axis denote the days of observations shown in panels A and B. Clearly visible in the bottom panel are periodicities in the density amplitudes of around 5 days, suggesting a modulation of the gravity waves by a 5-day oscillation in the atmosphere. Red crosses in the same panel are temperatures at each flyby, normalised to the average value $T_{av} = 114$ K. These show a periodicity of between 3–7 days. Previously, cloud tracking near 65 km altitude from ground based telescopes and from

spacecraft have been the primary method of detecting waves in Venus' atmosphere[11,12], alongside some measurements of thermal emissions above (65–90 km)[13,14]. These overall suggested the presence of a 4-day Kelvin wave at low latitudes and of a Rossby wave at 5-6 day period at mid to high latitudes[11,14]. More recently, radar tracking of the Magellan spacecraft revealed the presence of a 9-day oscillation near the equator (11°N) at 164–184 km altitude[2]. The latter was interpreted as possibly originating from nonlinear wave-wave interaction between two planetary waves occurring near the cloud top[2]. The modulation of gravity waves by planetary waves was shown to be important on Earth to explain planetary wave periodicities detected in the thermosphere/ionosphere system[15], and our findings suggest the same to occur on Venus. Our observation of a high latitude 5-day modulation of gravity wave amplitudes at 130-140 km may thus be linked to the previous detection of a high latitude quasi 5-day oscillation at 65–90 km[13,14]. The planetary wave may have interacted non-linearly with the gravity waves near 65–90 km, modulating their amplitudes and enabling the 5-day periodicity to be carried into the thermosphere.

Unlike the density perturbations, the temperature oscillations in Figure 3 are not signatures of modulated small scale temperature waves but periodic changes of the mean temperature itself with an amplitude of $\sim$20% ($\sim$22 K). Since we are sampling temperatures within a narrow longitude range (220–242°) this oscillation could either represent the reappearance of a warmer region advected around the planet by a super-rotating atmosphere, or it may be interpreted as a planetary wave. The upward propagation of planetary waves into the thermosphere is strongly affected by zonal wind speeds, being prevented from passing through a level where the zonal wave phase and mean zonal wind speed are equal. Zonal winds have been observed in the 90–120 km regime via

Doppler shifts of the CO_2 10μm emission line (from 110$\pm$10 km)[16] as well as CO sub-mm absorption lines (from 90–115 km)[17]. Dynamics in that regime are found to be highly variable, transitioning from a region near the cloud top (65 km) dominated by retrograde super-rotating zonal (westward) (RSZ) flow ($v \leq$100 m/s) to sub-solar to anti-solar (SS-AS) circulation ($v \leq$150 m/s) which is thought to become important in the thermosphere above $\sim$150 km[16–18]. The exact balance of the RSZ and SS-AS components changes with time and altitude and is unknown above $\sim$130 km altitude. While previous studies have shown that some Rossby waves can propagate vertically into the lower thermosphere[11,19], the variability of zonal winds and our inability from the limited dataset to better characterise the horizontal structure and possible propagation speed of the temperature oscillations prevents us from assessing whether or not we are seeing a planetary wave in the temperatures. The other possible explanation is that of a long-lived temperature structures being advected around the planet by zonal winds. At 75° latitude a 5 day periodicity is produced by a $\sim$23 m/s zonal wind, indicating a weak RSZ speed, consistent with some of the ground based observations[16,17,20].

Figure 4 is a visualisation of the atmospheric gravity waves versus latitude and longitude, the contours being the normalised wave perturbations, $(\rho - \rho_{fit})/\rho_{fit}$. Panel (a) shows the observations, with overdrawn black lines representing the spacecraft trajectories. Panels (b)–(d) are wave fits, the sum of both wave trains (b) and wave trains 1 (c) and 2 (d) individually. While the underlying observations were carried out at different longitudes, they were also made on different days, so the longitude variations can also be regarded as time variations. By comparing panels (a) and (b), we see that the wave fits capture well the overall observed structures. From panel (c) we cannot

identify phase propagation of wave 1 but panel (d) suggests that wave 2 may exhibit a moderate southward phase propagation. The dashed and dotted lines illustrate two possible options of linking wave fronts and thus determining phase speeds. These suggest meridional speeds of around 0.1 m/s (dotted lines) and 0.5 m/s (dashed lines). Despite the ambiguity in the meridional phase speed, the value is likely not to exceed the larger of both, so wave 2 appears to be quasi–stationary.

The Venus Express Visible and Infrared Thermal Imaging Spectrometer-Mapper (VIRTIS-M) remotely observed 4.3 μm emissions from 110–140 km altitude and discovered wave structures with horizontal wavelengths of around 90–400 km and meridional propagation speeds of around 30 m/s [21]. Both our λ_1 and λ_2 values are comparable to those values but the phase propagation speed of wave 2 appears to be much lower. Given our limited latitude window and 1–day time resolution of observations, during which time a 30 m/s wave will have propagated by 24° latitude, we cannot capture the phase propagation of the waves identified by VIRTIS-M. The apparent randomness of wave 1's phase in panel (c) is not inconsistent with waves found by those observations, we may thus have sampled *in-situ* the same waves identified remotely by VIRTIS-M. Our findings illustrate the significant influence of Venus' cloud top layer on its lower thermosphere, emphasising the importance of understanding vertical coupling in Venus' atmosphere.

Methods

The VEx inertial measurement package contains 3 Honeywell QA-2000 accelerometers which provide 8 Hz velocity increment data. The measured acceleration, in absence of thrusts and after removal of angular accelerations and with Solar radiation pressure being negligible for altitudes

below 150 km, is due to atmospheric drag. Details pertaining to the derivation of densities from accelerometer measurements were previously presented [22,23]. We processed the 8 Hz accelerometer data with the Geodesy by Simultaneous Numerical Integration (GINS) software which calculates satellite orbits by taking into account all gravitational and non-gravitational forces acting on the satellite[10]. This data processing produced atmospheric densities at 1 Hz sampling.

The uncertainty in derived densities is the sum of a systematic part of 10% due to the uncertainty in the satellite drag coefficient, C_D=2.60$\pm$0.26[24] and a variable noise and bias part due to the accelerometers. The systematic error does not affect analyses of relative variations such as wave perturbations. The uncertainty due to the computed drag area and mass of the spacecraft is negligible thanks to accurate knowledge of its attitude and mass. The (formal) noise of the accelerometers, after 16-point smoothing and differencing the velocity increments one second apart, is 0.001 m/s^2 (1-σ). A signal-to-noise (1σ) ratio of one is reached on average at 139 km altitude, which corresponds to profiles of about 80 s duration.

Another way of evaluating the validity range of the VEx densities is by means of comparison with a model. The VEx-to-VTS3 density ratios were computed for each profile. The density ratios start to present a typical noise behaviour for altitudes consistent with those calculated applying the formal accelerometer noise (see bottom panel of Figure 1).

1. Forbes, J. M.. Wave coupling in terrestrial planetary atmospheres, in: *Atmospheres in the Solar*

System: Comparative Aeronomy, edited by M. Mendillo, A. Nagy, and J. H. Waite, *Geophys. Monogr. Ser.*, **130**, 171–190, AGU, Washington, D. C. (2002).

2. Forbes, J. M. & A. Konopliv. Oscillation of Venus' upper atmosphere, *Geophys. Res. Lett.*, **34**, L08202 (2007)

3. Yelle, R. V. & S. Miller. Jupiter's thermosphere and ionosphere, in *Jupiter. The planet, satellites and magnetosphere*, edited by F. Bagenal, T. E. Dowling, W. B. McKinnon, 185–218, Cambridge University Press, Cambridge, UK (2004).

4. Müller-Wodarg, I. C. F & R. V. Yelle. Waves and horizontal structures in Titan's thermosphere, *J. Geophys. Res.*, **111**, A12315 (2006).

5. Müller-Wodarg, I. C. F., J. M. Forbes & G. M. Keating. The thermosphere of Venus and its exploration by a Venus Express Accelerometer Experiment. *Planet. & Sp. Sci.*, **54**, 1415–1424 (2006).

6. Hedin, A. E., Niemann, H. B., Kasprzak, W. T. & A. Seiff. Global Empirical Model of the Venus Thermosphere. *J. Geophys. Res.*, **88**, 73–83 (1983)

7. Niemann, H. B., Kasprzak, W. T., Hedin, A. E., Hunten, D. M. & Spencer, N. W.. Mass spectrometric measurements of the neutral gas composition of the thermosphere and exosphere of Venus. *J. Geophys. Res.*, **85**, 7817–7827 (1980).

8. Mahieux, A., Vandaele, A. C., Robert, S., Wilquet, V., Drummond, R., López Valverde, M. A., López Puertas, M., Funke, B. & J. L. Bertaux. Rotational temperatures of Venus upper

atmosphere as measured by SOIR on board Venus Express. *Planet. & Sp. Sci.*, **113-114**, 347–358 (2015).

9. Piccialli, A., Montmessin, F., Belyaev, D., Mahieux, A., Fedorova, A., Marcq, E., Bertaux, J.-L., Tellmann, S., Vandaele, A.C. & O. Korablev. Thermal structure of Venus nightside upper atmosphere measured by stellar occultations with SPICAV/Venus Express, *Planet. & Sp. Sci.*, **113-114**, 321–335 (2015).

10. Rosenblatt, P., S. L. Bruinsma, I. C. F. Müller-Wodarg, B. Häusler, H. Svedhem, and J. C. Marty. First ever *in-situ* observations of Venus' polar upper atmosphere density using the tracking data of the Venus Express Atmospheric Drag Experiment (VExADE). *Icarus*, **217**, 831–838 (2012).

11. Del Genio, A. D., & W. B. Rossow, Planetary-scale wave and the cyclic nature of cloud top dynamics on Venus, *J. Atmos. Sci.*, **47**, 293–318 (1990).

12. Rossow, W. B., A. D. Del Genio, & T. Eichler. Cloud-tracked winds from Pioneer Venus OCPP images. *J. Atmos. Sci.*, **47**, 2053–2084 (1990).

13. Apt, J., R. A. Brown & R. Goody. The Character of the Thermal Emission from Venus, J. Geophys. Res., **85**, 7934–7940 (1980).

14. Apt, J., & J. Leung, Thermal periodicities in the Venus atmosphere, *Icarus*, **49**, 423–427 (1982).

15. Meyer, C. K.. Gravity wave interactions with mesospheric planetary waves: A mechanism for penetration into the thermosphere-ionosphere system. *J. Geophys. Res.*, **104**, 28,181–28,196 (1999).

16. Sornig, M., G. Sonnabend, D. Stupar, P. Kroetz, H. Nakagawa & I. C. F. Mueller-Wodarg. Venus upper atmospheric dynamical structure from ground-based observations shortly before and after Venus inferior conjunction 2009, *Icarus*, **225**, 828–839 (2013).

17. Clancy, R. T., B. J. Sandor, & G. Moriarty-Schieven. Circulation of the Venus upper mesosphere/lower thermosphere: Doppler wind measurements from 2001–2009 inferior conjunction, sub-millimeter CO absorption line observations, *Icarus*, **217**, 794–812 (2012).

18. Bougher, S. W., S. Engel, R. G. Roble & B. Foster. Comparative terrestrial planet thermospheres: 2. Solar cycle variation of global structure and winds at equinox, *J. Geophys. Res.*, **104**, 16591–16611 (1999).

19. Kouyama, T., T. Imamura, M. Nakamura, T. Satoh & Y. Futaana. Vertical propagation of planetary-scale waves in variable background winds in the upper cloud region of Venus. *Icarus*, **248**, 560–568 (2015).

20. Schmuelling, F., J. Goldstein, T. Kostiuk, T. Hewagama & D. Zipoy. High precision Wind measurements in the upper Venus atmosphere. *Bulletin of the Amer. Astron. Soc.*, **32**, 1121 (2000).

21. Garcia, R. F., P. Drossart, G. Piccioni, M. López-Valverde & G. Occhipinti. Gravity waves in the upper atmosphere of Venus revealed by CO_2 nonlocal thermodynamic equilibrium emissions. *J. Geophys. Res.*, **114**, E00B32 (2009).

22. Bruinsma, S. L., D. Tamagnan & R. Biancale. Atmospheric densities derived from CHAMP/STAR accelerometer observations. *Planet. Space Sci.*, **52**, 297–312 (2004).

23. Bruinsma, S., J. M. Forbes, S. Nerem & X. Zhang, Thermosphere density response to the 20-21 November 2003 solar and geomagnetic storm from CHAMP and GRACE accelerometer data. *J. Geophys. Res.*, **111**, A06303 (2006).

24. Arona, L., M. Muller, G. Huguet, I. Tanco & N. Keil. Venus Express solar arrays rotation experiments to measure atmospheric density. *J. Aerosp. Eng., Sci. & Appl.*, **IV**, 68–81 (2011).

Acknowledgements SB and JCM thank CNES/TOSCA for their support.

Author contributions I. M-W carried out the density wave extraction and analysis shown in Figures 2–4, and jointly with S. B. led the scientific interpretation of the results. S. B. and J.-C. M. performed the analysis of raw accelerometer readings using the GINS software in order to obtain density values. S. B. carried out the error analysis which led to Figure 1. H. S. led the implementation of the VExADE experiment in the mission planning and made important scientific contributions in the interpretation of the data. I.M-W wrote the paper with significant contributions from all the authors in interpreting the results and editing of the manuscript.

Competing Interests The authors declare that they have no competing financial interests.

Correspondence Correspondence and requests for materials should be addressed to I.M-W. (email: i.mueller-wodarg@imperial.ac.uk).

Figure 1 Densities in Venus' upper atmosphere. The upper panel shows measurements along spacecraft trajectories for each of the 18 flybys during the aerobraking campaign of Venus Express from June 24–July 11, 2014 at 130–140 km altitude. Red dashed lines are examples of best fit background hydrostatic density profiles. The middle panel shows normalised perturbations around background values, illustrating considerable abundance of atmospheric waves. The bottom panel illustrates that the noise level of data outside of our chosen data window (below 71.5°N and above 79.0°N) increases considerably, justifying our chosen range of science data.

Figure 2 Density profiles in Venus' lower thermosphere. Black symbols denote individual densities measured with Venus Express Aerobraking between June 24 and July 11, 2014, the red crosses are binned average values and their 1-σ variability within bins spaced vertically by 2.5 km. The red line denotes an average density profile with a slope (scale height H) determined from best hydrostatic fits for each flyby. Blue crosses are averages of individual densities from the VTS3 model[6] extracted at the same locations as observed densities. The VTS3 averages are extracted within the identical bins as Venus Express measurements, but for clarity the blue crosses have been shifted downward by 0.2 km in the figure.

Figure 3 Atmospheric waves on Venus. Wave–like perturbations are shown for two flybys on June 30 (panel A) and July 07, 2014 (panel B). Dashed lines are fits to the density

perturbations with two wave trains. The bottom panel shows in blue the normalised amplitudes, $A/A_{\rm mean}$, of wave train 1 (dots) and 2 (triangles) versus days of observation. The blue line shows the average of these two amplitudes, indicating a 5-day modulation. Mean amplitudes over the 18 days are $A_{1\ \rm mean} = 0.09$ and $A_{2\ \rm mean} = 0.07$. Red crosses and the red line in the bottom panel are normalised temperatures, $T/T_{\rm mean}$, with the mean value $T_{\rm mean} = 114$ K.

Figure 4 Maps of density waves in Venus' lower thermosphere. Panel (a) shows the VExADE observations, (b) are best fits with two wave trains '1' and '2', shown individually in panels (c) and (d), respectively. Solid lines in panel (a) are the VEx trajectory paths mapped onto the surface. The dotted and dashed lines in panel (d) illustrate possible southward phase propagation of wave 2 at meridional speeds of 0.1 m/s and 0.5 m/s, respectively.

Figure 1

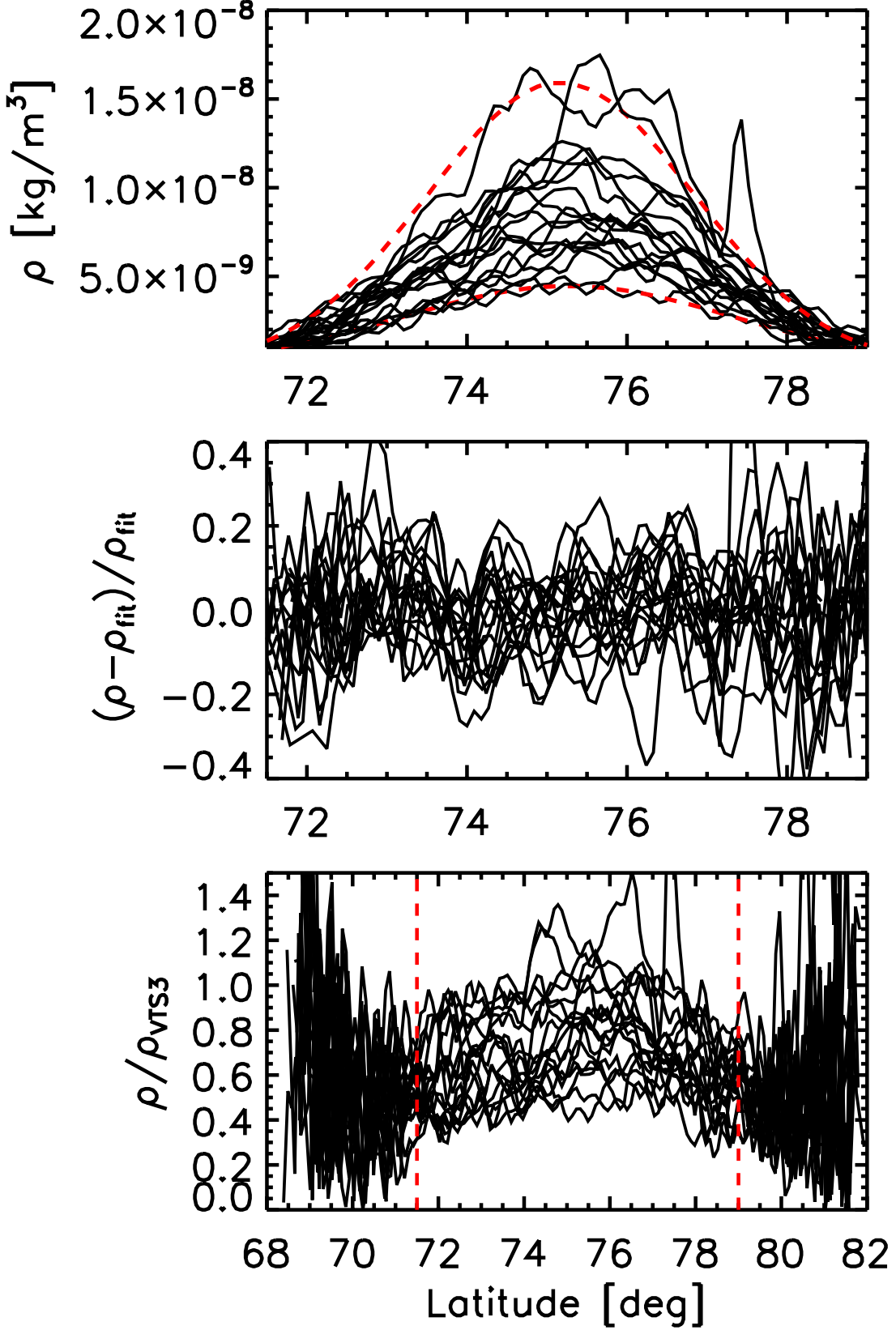
ρ [kg/m³]
2.0×10⁻⁸
1.5×10⁻⁸
1.0×10⁻⁸
5.0×10⁻⁹
72
74
76
78
(ρ−ρfit)/ρfit
0.4
0.2
0.0
−0.2
−0.4
ρ/ρVTS3
1.4
1.2
1.0
0.8
0.6
0.4
0.2
0.0
68
70
72
74
76
78
80
82
Latitude [deg]

Figure 2

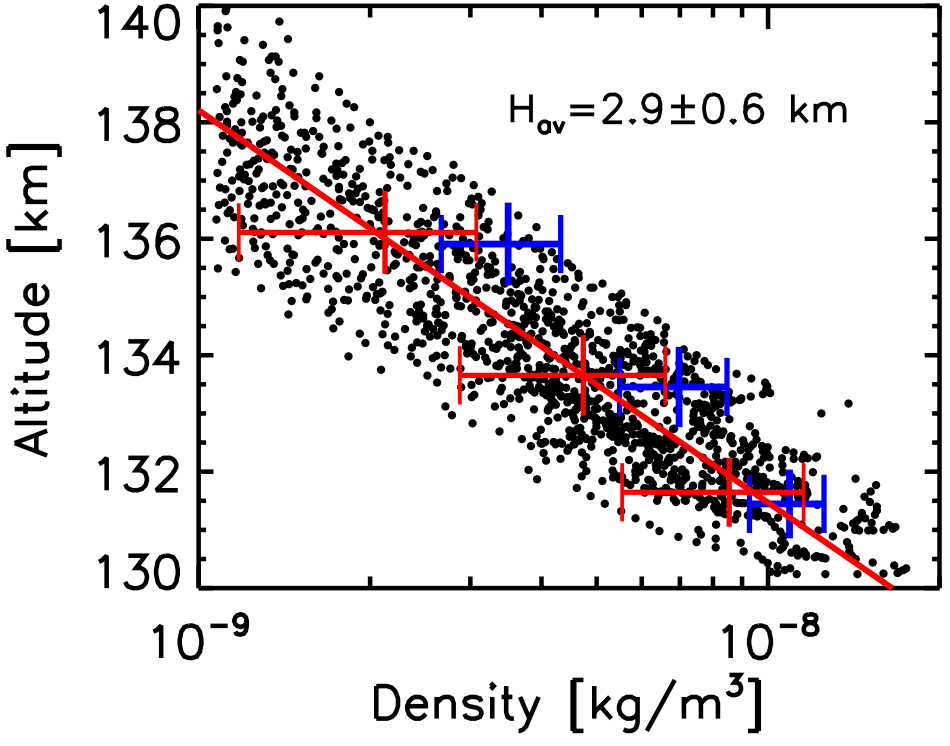
140
138
136
134
132
130
Altitude [km]
H_{av}=2.9±0.6 km
10^{-9}
10^{-8}
Density [kg/m^3]

Figure 3

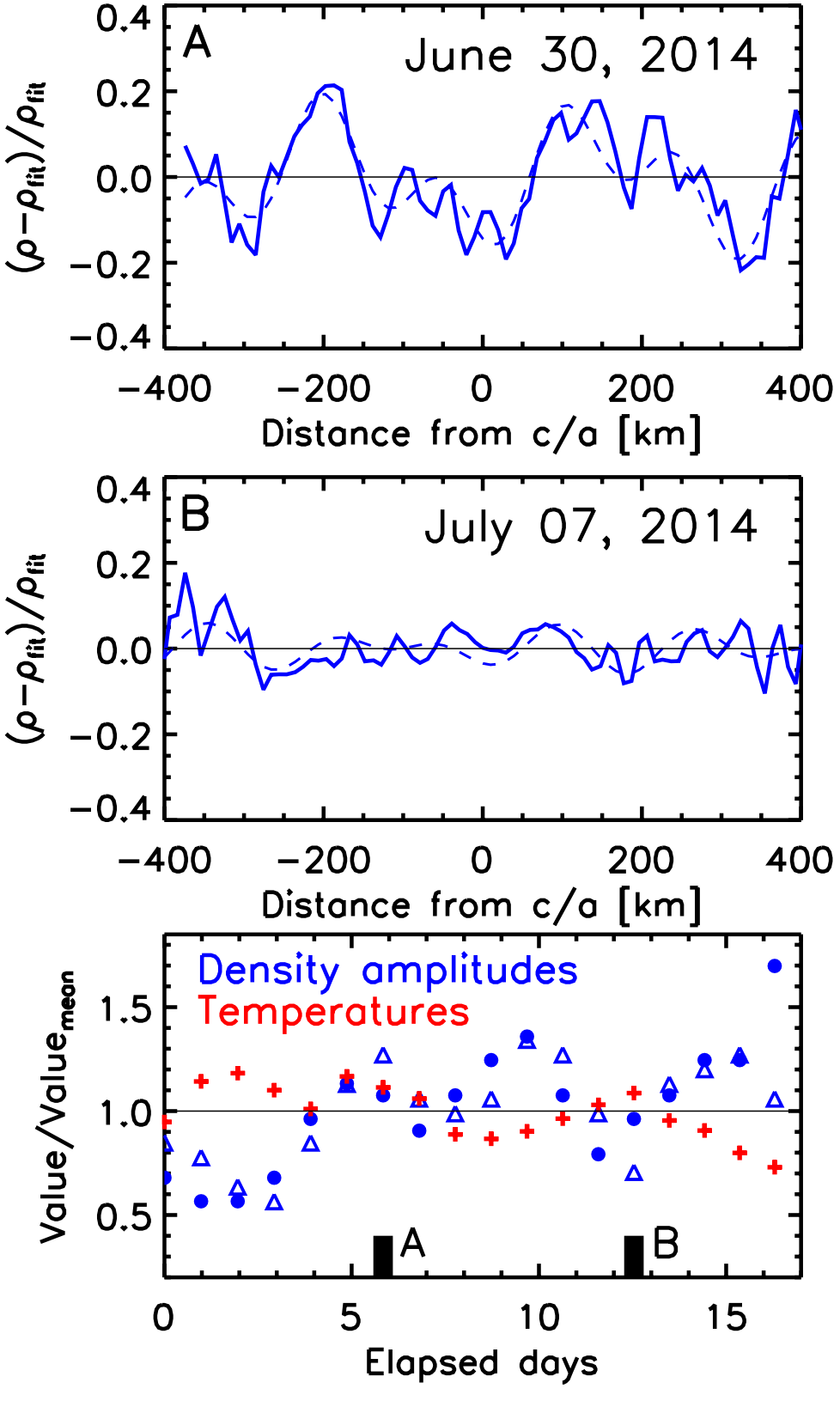
A
June 30, 2014
$(\rho-\rho_{fit})/\rho_{fit}$
0.4
0.2
0.0
−0.2
−0.4
−400
−200
0
200
400
Distance from c/a [km]
B
July 07, 2014
$(\rho-\rho_{fit})/\rho_{fit}$
0.4
0.2
0.0
−0.2
−0.4
−400
−200
0
200
400
Distance from c/a [km]
Density amplitudes
Temperatures
Value/Value$_{mean}$
1.5
1.0
0.5
A
B
0
5
10
15
Elapsed days

Figure 4

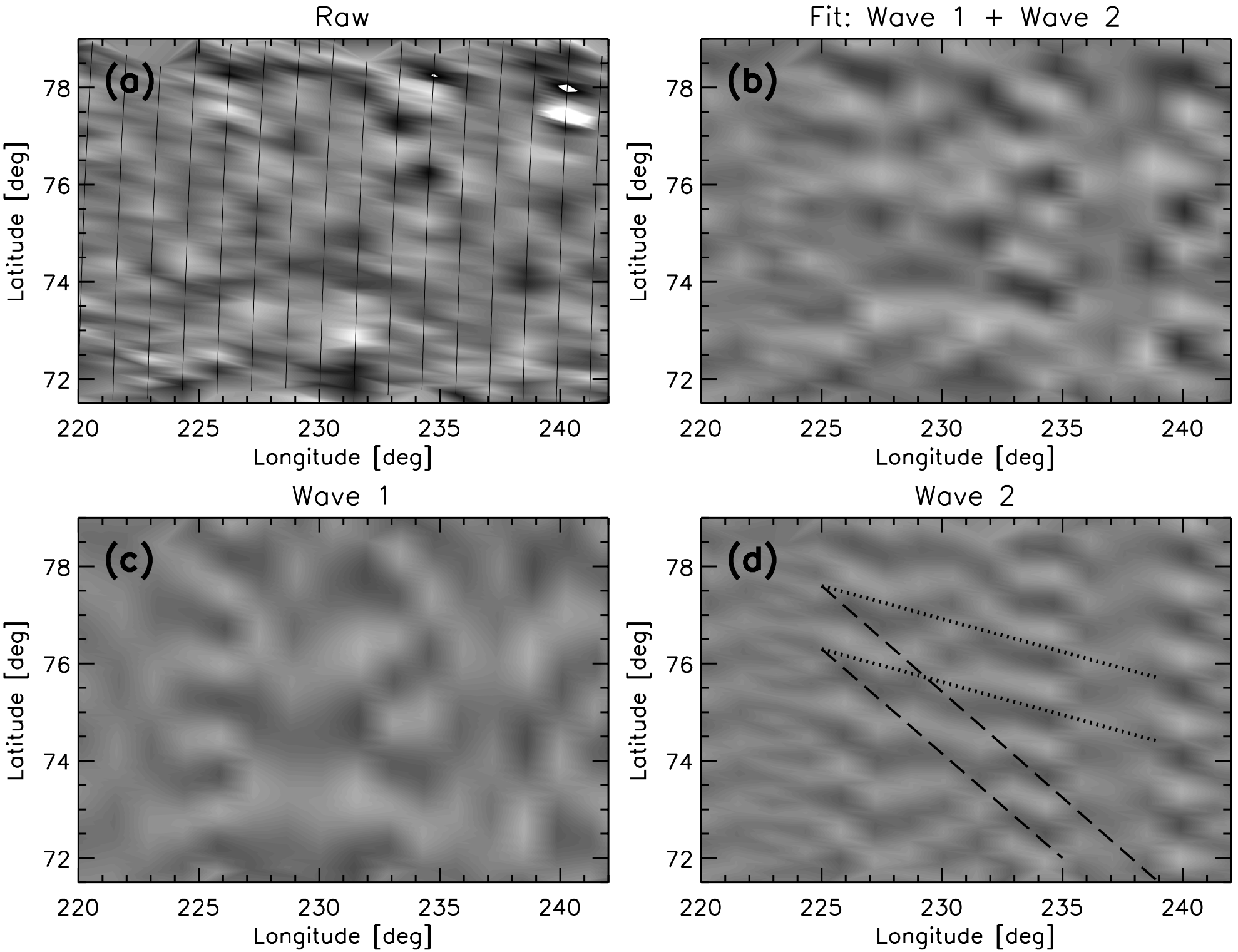
Raw
(a)
Fit: Wave 1 + Wave 2
(b)
Wave 1
(c)
Wave 2
(d)
Latitude [deg]
Longitude [deg]
72
74
76
78
220
225
230
235
240